

Neural 5G Indoor Localization with IMU Supervision

Aleksandr Ermolov*, Shreya Kadambi[†], Maximilian Arnold*, Mohammed Hirzallah[†],
Roohollah Amiri[†], Deepak Singh Mahendar Singh[†], Srinivas Yerramalli[†],
Daniel Dijkman*, Fatih Porikli[†], Taesang Yoo[†], Bence Major*
*Qualcomm Technologies Netherlands B.V., [†]Qualcomm Technologies Inc.
{aermolov,skadambi,marnold,bence}@qti.qualcomm.com

Abstract—Radio signals are well suited for user localization because they are ubiquitous, can operate in the dark and maintain privacy. Many prior works learn mappings between channel state information (CSI) and position fully-supervised. However, that approach relies on position labels which are very expensive to acquire. In this work, this requirement is relaxed by using pseudo-labels during deployment, which are calculated from an inertial measurement unit (IMU). We propose practical algorithms for IMU double integration and training of the localization system. We show decimeter-level accuracy on simulated and challenging real data of 5G measurements. Our IMU-supervised method performs similarly to fully-supervised, but requires much less effort to deploy.

Index Terms—5G, Localization, Positioning, IMU, self-supervised

I. INTRODUCTION

This work is focused on the localization task, i.e. locating the user equipment (UE) in some specific indoor environment from available measurements. Such methods can be classified based on input modalities: light detection and ranging (Lidar) measurements, visual observations, inertial measurement unit (IMU), radio signal. The latter is of particular interest [1] due to the widespread use of the technology and its privacy-preserving properties.

Radio signal localization is a well-known task, where time of flight of radio signals from the transmitter to the receiver is measured to derive the user location. This requires either synchronization at the network side (for downlink or uplink time difference of arrival, i.e., DL-TDOA and UL-TDOA), bi-directional signaling used for round-trip time-based measurements (i.e., RTT) or angle-based estimates (Angle of Departure, AoD or Angle of Arrival, AoA) if multiple antennas are available. Fundamentally, all these methods assume the presence of Line-of-Sight (LoS) in the observed channel. If excess of measurements are present, outlier rejection methods can be employed to reduce the impact of non-Line of Sight (NLoS) measurements on the final positioning accuracy.

In recent literature, supervised machine learning methods [2]–[6] have been proposed for dealing with challenging LoS conditions. These methods train an algorithm to learn a mapping from the observed *Channel State Information (CSI)* of multiple cells to the coordinates at which the CSI is measured. Training such algorithms generally requires collecting CSI from the target environment densely along with the user

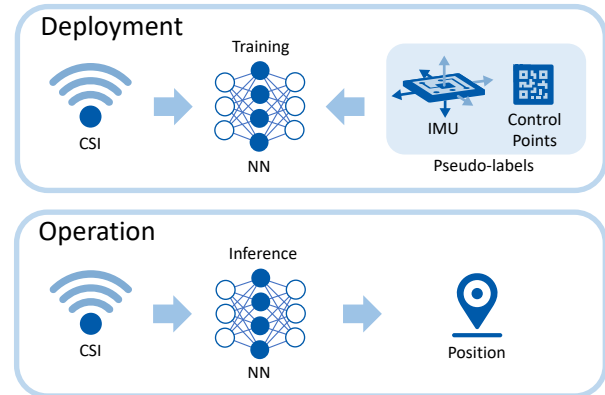


Fig. 1. Two stages of our method. Note that during operation the position prediction does not depend on past or future steps, only observed CSI is used.

location. Acquiring such precise positioning labels requires a careful measuring process, which makes this approach somewhat impractical to deploy. This limitation has given rise to semi-supervised and unsupervised learning methods [7]–[12].

The availability of CSI, which contains implicit information about the radio environment and spatial geometry of the users has enabled *Channel Charting* methods [7] to learn a low dimensional representation from CSI that still preserves the time-varying and space-varying components in an unsupervised fashion. However, these methods still require samples with known labels to accurately predict the location of the user from learned low-dimensional representation.

IMU measurements do not depend on expensive or privacy-breaching sensors, but positions, obtained from IMU integration, are drifting over time, accumulating the error. There are several very recent works that suggest to combine radio and IMU modalities [13]–[16]. Our work continues this line of research. In this proposal, we significantly relax the requirement of dense position labels, by replacing the manual position measurement process with automatically obtained “pseudo-labels”. Such pseudo-labels could be acquired using sensors such as a vision camera or Lidar, but such system generally have a higher cost and are not privacy-preserving. Our solution acquires these pseudo-labels from IMU measurements.

In summary, our contributions are the following:

- We propose a neural network (NN) based positioning system trained on pseudo-labels, obtained from IMU double integration.
- To improve pseudo-labels accuracy, we propose trajectory fitting algorithm, which combines IMU dead-reckoning with limited control point information.
- We demonstrate that IMU trajectory fitting can be iteratively refined using CSI information further improving the accuracy.
- We prototype our solution on a simulated dataset and then verify the takeaways with a real data collection setup. The model shows decimeter-level accuracy while using only single control point and noisy IMU measurements during deployment.

II. METHOD

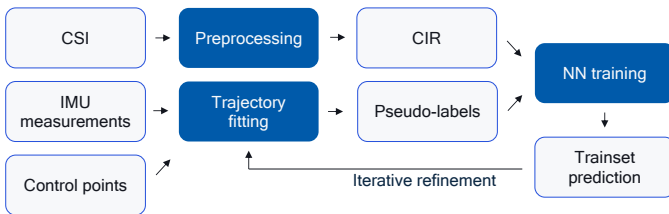


Fig. 2. Training pipeline.

The positioning solution consists of two stages: deployment and operation (Fig. 1). At the deployment stage, the UE moves throughout the environment, with the CSI and IMU measurements collected. A few prominent points on the ground are marked with fiducials. At these points, the coordinates and corresponding velocities are computed using a privacy-preserving floor-facing camera. These points are the *control points*. An automated process then computes the pseudo-label coordinates for the remaining points, by finding a most likely trajectory, derived from IMU measurements passing through control points. The last step of deployment is training a neural network for each time step to predict from the CSI of that time step the pseudo-label position. At operation time, the CSI is fed to the neural network, which estimates the UE position. Note that the control points with floor-facing camera and IMU measurements are only used during deployment, and *only* CSI is required during operation.

Our training pipeline consists of several stages (Fig. 2). First, we preprocess the raw CSI information. Next, we compute pseudo-labels from IMU measurements and control points. After that, we train the NN using obtained information. Finally, we refine the pseudo-labels and retrain the NN.

A. Preprocessing

For a real data collection setup, channel state information is measured on the uplink at the transmission-reception-points (TRPs). For all our results we are using 5G numerology for the industry case, where we measure using a bandwidth of 100MHz, a subcarrier spacing of 30kHz the channel frequency response at the pilot locations. Thus only each fourth subtone

is occupied. The channel impulse response is created by calculating the inverse Fourier transformation on these down-sampled subtones.

As mentioned in the section on the data set, since UE and TRPs are not synchronized we compensate for the drift in the pre-processing. The group delay offset is correct for when the measurements are collected.

1) *LoS peak Alignment*: For real data, inspired from classical time-difference-of-arrival estimation techniques, one can remove the arbitrary time/phase shift of the transmit starting time, via LoS peak alignment. To compensate for the clock offset drift we align the line of sight peaks of a reference antenna. A showerhead TRP₀ provides a good LoS path across most of the trajectory, antenna 0 of TRP₀ is chosen as a reference.

For each CSI packet, the first measured peak of the reference antenna T_0 is shifted to arrive at a fixed time step T_{bin} . If the peak is not found, dataset median peak is used as a fallback. The effect of peak alignment can be seen in the Fig. 3. For the rest of the TRPs and antennas, channel impulse response (CIR) is shifted by the same amount $T_{\text{bin}} - T_0$.

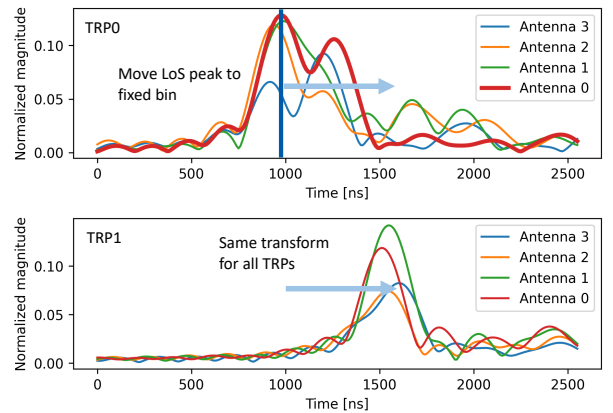


Fig. 3. LoS alignment procedure. The LoS peak is detected and CIR is rolled to align the peak to a specific bin. The same shift applies to all TRPs and antennas.

2) *Processing in time domain*: We obtain the SNR information for each antenna by computing the power on the pilot symbols and noise on the non-reference symbols. Before training, we remove samples with SNR below a threshold and normalize the time domain response per antenna.

B. Forward-backward algorithm

IMU data includes linear acceleration, angular velocity and device orientation. We assume that the sensor orientation is calibrated and we use global acceleration, obtained from it, to recover positions.

The key idea of the algorithm is to fit the trajectory of the UE between two control points using IMU data for each step. The algorithm takes as input: Δt_i — time difference between steps, $\mathbf{a}_i^{\text{IMU}}$ — noisy acceleration obtained from IMU, positions and velocities in control points $(\mathbf{x}_0^F, \mathbf{v}_0^F, \mathbf{x}_N^B, \mathbf{v}_N^B)$.

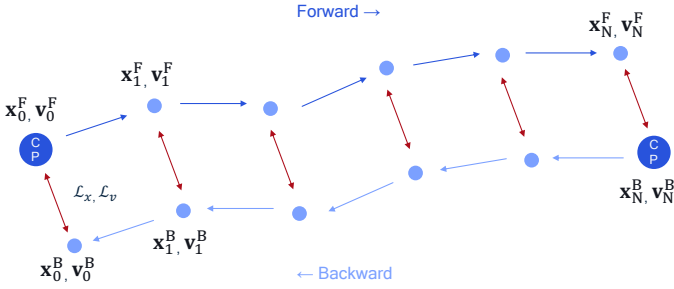


Fig. 4. Forward-backward algorithm. The scheme depicts the trajectory fitting based on misalignment of the positions obtained with forward and backward integration passes. Respectively, each position of the trajectory is represented with two points. We optimize the correction of the acceleration in each position pulling these two points to each other (shown with red arrow).

The trajectory positions can be recovered with double integration (dead-reckoning):

$$\begin{aligned} \mathbf{v}_n^{\text{IMU}} &= \mathbf{v}_{n-1}^{\text{IMU}} + \mathbf{a}_n^{\text{IMU}} \Delta t_n, \\ \mathbf{x}_n^{\text{IMU}} &= \mathbf{x}_{n-1}^{\text{IMU}} + \mathbf{v}_n^{\text{IMU}} \Delta t_n \end{aligned} \quad (1)$$

For each step, we train a correction parameter $\mathbf{a}_n^{\text{cor}}$ that compensates the noise drift. Resulting acceleration $\tilde{\mathbf{a}}_n = \mathbf{a}_n^{\text{IMU}} + \mathbf{a}_n^{\text{cor}}$. In this case, forward and backward integration:

$$\mathbf{v}_n^{\text{F}} = \mathbf{v}_{n-1}^{\text{F}} + \tilde{\mathbf{a}}_n \Delta t_n, \quad \mathbf{x}_n^{\text{F}} = \mathbf{x}_{n-1}^{\text{F}} + \mathbf{v}_n^{\text{F}} \Delta t_n \quad (2)$$

$$\mathbf{v}_{n-1}^{\text{B}} = \mathbf{v}_n^{\text{B}} - \tilde{\mathbf{a}}_n \Delta t_n, \quad \mathbf{x}_{n-1}^{\text{B}} = \mathbf{x}_n^{\text{B}} - \mathbf{v}_n^{\text{B}} \Delta t_n \quad (3)$$

Finally, our optimization losses:

$$\begin{aligned} \mathcal{L}_x &= \sum_i \|\mathbf{x}_i^{\text{F}} - \mathbf{x}_i^{\text{B}}\|_2^2 \\ \mathcal{L}_v &= \sum_i \|\mathbf{v}_i^{\text{F}} - \mathbf{v}_i^{\text{B}}\|_2^2 \\ \mathcal{L}_{\text{reg}} &= \sum_i \|\mathbf{a}_i^{\text{cor}}\|_2^2 \end{aligned} \quad (4)$$

\mathcal{L}_x and \mathcal{L}_v optimize $\mathbf{a}_n^{\text{cor}}$ such that forward and backward integrations produce close trajectories. At the same time, \mathcal{L}_{reg} pushes the correction to be as small as possible, assuming that the IMU noise is zero-centered. The scheme of the algorithm is depicted on Fig. 4. An example of forward integration, backward integration and correction is shown on Fig. 5. The pseudo-labels are generated as the average position of the forward and backward passes after correction.

C. Iterative refinement algorithm

In some cases, the accuracy of the trained NN can surpass the accuracy of IMU pseudo-labels. E.g., it is a common situation when the density of train samples is high and the network is trained on many close-by samples with different label errors. In such cases, the network can generalize well reducing these errors. As a result, the network can be used to refine IMU trajectory fitting. The complete algorithm:

- 1) Create pseudo-labels with forward-backward algorithm.
- 2) Initialise the network randomly, train on pseudo-labels.
- 3) Predict positions for training set $\mathbf{x}_i^{\text{Model}}$ using the trained network.

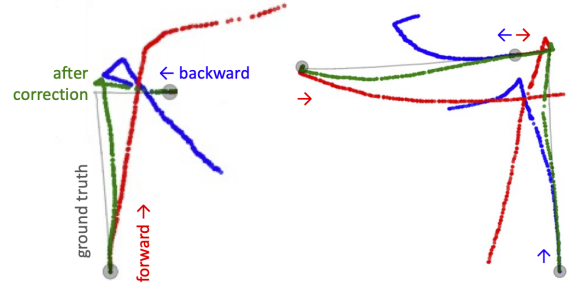


Fig. 5. Simulated trajectories. Gray circles show control points, which act as starting points for integration. Red and blue trajectories are obtained with forward and backward integration. They quickly diverge from the ground truth due to the error accumulation. Green trajectory is the result of the forward-backward algorithm, it corrects the error pushing the trajectory closer to the ground truth.

- 4) Create pseudo-labels with forward-backward algorithm and predictions. In this case, the forward-backward scheme includes additional prediction point (positions from the previous step) and \mathcal{L}_x is calculated between positions $\mathbf{x}_i^{\text{F}}, \mathbf{x}_i^{\text{Model}}$ and $\mathbf{x}_i^{\text{B}}, \mathbf{x}_i^{\text{Model}}$ (Fig. 6).
- 5) Go to point 2 until convergence.

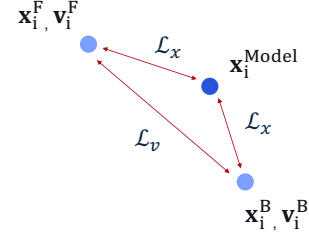


Fig. 6. Iterative refinement losses. The algorithm extends the scheme 4 with model prediction point $\mathbf{x}_i^{\text{Model}}$, and points, obtained from integration, are pulled to it.

III. EXPERIMENTAL SETUP

In this section we discuss our experimental setup including the datasets. We start with a simulated environment, used for prototyping the solution. Next, we present real warehouse-like setup, used to verify our takeaways.

A. Simulated dataset

We use an indoor floorplan $30 \text{ m} \times 20 \text{ m}$ (Fig. 7) to create a simulated dataset using Wireless-Insite by RemCom [17]. In order to maintain realistic propagation characteristics we setup walls with different material properties. All inner walls were made of dielectric with strong permittivity $\epsilon = 2.8$. Outer walls along with the floor and ceiling were made of concrete with a thickness of 30 cm and permittivity of $\epsilon = 5.31$. The doors are mostly free space however, the outer wall doors are configured with a glass material with $\epsilon = 2.4$. The transmitter and receiver antennas are configured with omnidirectional half-wave dipoles. Three access points are configured as receivers at a height of 3 m while the UEs are located at 1 m height allowing only a subset of trajectories

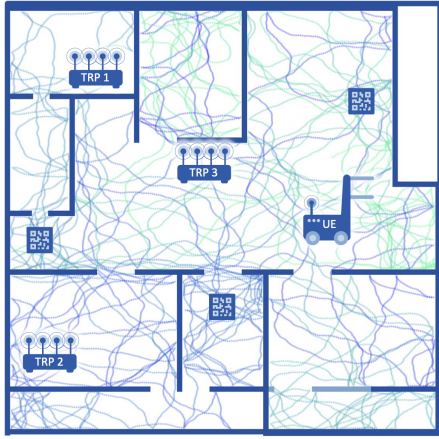


Fig. 7. Data simulation. 30 m \times 20 m environment with 3 TRPs and 3 control points (QR codes on the floor). Colored background curve shows the trajectory of the UE, used for the experiment.

to lie in the LoS region. We currently run X3D ray tracing method of Wireless Insite allowing each ray to undergo up to 1 diffraction, 2 transmissions, and 4 reflections. Wireless-Insite output is further bandlimited to 100 MHz with subcarrier spacing at 30 kHz and with 3264 subcarriers. We generate trajectories with a random walk. We randomly split samples into train and test sets (90% and 10%). The total number of samples is 8982 with a 20 cm step size.

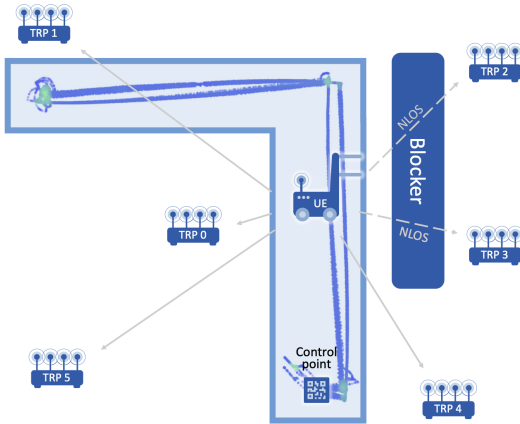


Fig. 8. Warehouse dataset. The actual UE trajectory is shown on background, green color highlights regions with high points density.

B. Warehouse dataset

The network is deployed consisting of 6 TRPs surrounding a region of interest. Each TRP is deployed with 4 antennas. Two antennas in each TRP are vertically polarized and the other two are horizontally polarized respectively. The antenna for TRP₀ is a showerhead antenna while others are directional. The positions of the TRPs are known. Signals from all TRPs and all antenna ports are transmitted simultaneously. Similarly to simulation, the measured CSI has 3264 tones with a sub-

carrier spacing of 30 kHz. Ground truth positions are obtained from laser pointers and QR codes.

Floor-plan: UE is allowed to traverse an L-shaped region of size 15 m \times 12 m as shown in the Fig. 8. A thin metal sheet blocker is placed on the side blocking the LoS from TRP₂ and TRP₃ while allowing the refraction from the edges to pass (Fig. 8). TRPs are mounted very close to the ceiling of the warehouse at a height of ≈ 4.5 m. UE has a single antenna. The total number of samples is 39425 for training and 2775 for testing. Average step size is 3.4 cm with 160 ms time difference. The data was collected over two days.

C. IMU data

We simulate IMU measurements for our experiments. First, we calculate ground truth velocity and acceleration using coordinates and timestamps from datasets. Next, we input this acceleration into imuSensor system (part of Sensor Models, Navigation Toolbox, MATLAB), the configuration is listed in Tab. III. The simulator outputs noisy acceleration, similar to smartphone-grade IMU¹ measurements.

D. Control points

Control point is a point in which we can measure the position and velocity with high precision. In real environment it can be implemented with a floor fiducial marker and floor-facing camera on the UE. Radius defines the area and actual positions covered with the control point, we use 20 cm in all experiments (if not otherwise specified). We use 3 control points in Simulated dataset (Fig. 7), and 1 in Warehouse (Fig. 8). Additionally, we use random control points in the ablation experiments IV-A4.

E. Implementation details

The localization model is a fully-connected neural network. It consists of three layers with 1024, 512 and 3 output size. We use hyperbolic tangent activation functions. Input data, represented with first 256 bins of CIR for each antenna and each TRP, flattened into one vector.

We use Adam optimizer with learning rate 0.0001 with 10 \times drop for last 50 epochs. We use batch size 256. We train for 600 epochs for supervised baseline, 100 epochs for the IMU-supervised experiments, 300 epochs for control points number ablations, 100, 200, 300 and 400 epochs for iterative refinement with respect to each iteration. Using fewer epochs for the noisy ground truth provides some regularization to prevent overfitting to label imperfections. The localization is trained with smooth L1 loss for predicted positions. For Warehouse dataset, we use Kalman smoother for positions during validation with default² configuration.

We augment our data during training to improve generalization. In case of pseudo-labels, we add a uniform noise from range $(-5, 5)$ centimeters to positions. For Warehouse dataset, we add jittering to CIR with a random horizontal shift from a range of $(-7, 7)$ of total 256 bins.

¹<https://www.bosch-sensortec.com/products/motion-sensors/imus/bmi270/>

²<https://pykalman.github.io/>

For IMU trajectory fitting, we use stochastic gradient descent with learning rate 0.0001. Correction parameters are initialized randomly from normal distribution with variance 0.0001 m s^{-2} . The total loss is a sum of three terms: $\mathcal{L} = \mathcal{L}_x + 10^3 \mathcal{L}_v + 10^4 \mathcal{L}_{\text{reg}}$, where the loss coefficients compensate magnitude difference of each term. The optimization is performed for 2000 steps.

IV. EXPERIMENTAL RESULTS

We present the horizontal absolute error in centimeters of the model on the test set for two datasets. Our IMU-supervised experiments are performed for 30 random seeds, and IMU noise is independently sampled over seeds; tables show mean value with standard deviation. For Simulated dataset, the area exceeds 500 m^2 inside a diverse environment, covered with only 3 TRPs, and our trajectory covers the area only partly. These challenges allow us to expand our findings to the real-case scenario. For Warehouse dataset, we have performed our experiments on measured 5G indoor data.

Tab. I includes fully-supervised baseline. In this case, we use all the ground-truth labels during training. This baseline provides an *upper bound* for our experiments, this accuracy can be obtained with perfect labels. Channel Charting baseline is provided for Warehouse dataset; for Simulated dataset this method was unable to learn the representation due to the sample sparsity. For this case, such type of methods requires additional heuristics [8].

Results include two versions of our method, with and without iterative refinement (IR). We can see that our IMU-supervised model is very close to the fully-supervised upper bound, and iterative refinement further reduces the gap. #CP column shows the number of control points for each method, the results confirm that our method reduces the deployment time effort. For more experiments on control points we refer to ablation studies IV-A4. Additionally, Fig. 9 demonstrates the performance of every iteration of the iterative refinement algorithm.

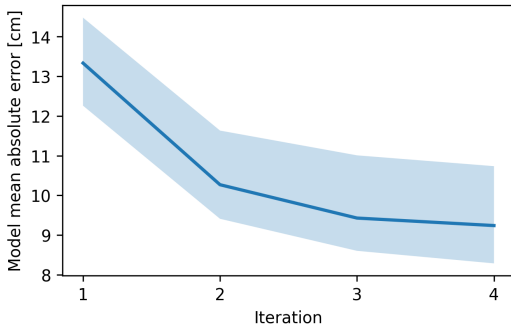


Fig. 9. Model accuracy on each iteration of the refinement procedure. The light area is 0.1 and 0.9 quantiles, the line is median for 30 seeds.

A. Ablation studies

The experiments in this section are performed on the Warehouse dataset.

TABLE I
HORIZONTAL ABSOLUTE ERROR [CM]

Method	#CP	Mean	Median	90 th perc.
Simulated dataset				
Fully-supervised	all	12.4	7.6	23.2
IMU-supervised	3	28.5 ± 3.2	21.3 ± 2.7	55.9 ± 8.5
IMU-supervised IR	3	20.1 ± 2.9	14.4 ± 2.0	40.1 ± 8.8
Warehouse dataset				
Fully-supervised	all	7.2	5.9	15.3
Channel Charting	32	30.9	26.8	108.5
IMU-supervised	1	13.4 ± 0.9	11.5 ± 0.7	25.0 ± 1.8
IMU-supervised IR	1	9.4 ± 1.0	8.4 ± 0.8	17.2 ± 2.3

TABLE II
IMU ABSOLUTE ERROR [CM]

Method	Mean	Median	90 th perc.
Dead-reckoning	110.9 ± 10.7	68.0 ± 9.0	285.3 ± 25.4
Forward-backward	17.8 ± 1.2	14.0 ± 1.3	41.0 ± 3.4

1) *IMU error*: IMU pseudo-labels are imprecise, and we can measure their error with respect to precise ground-truth. Tab. II includes two versions, basic dead-reckoning and integration with forward-backward correction. The dead-reckoning baseline demonstrates the IMU properties, and the corrected version shows the advantage of the correction algorithm. Additionally, we can see that the IMU-supervised model (Tab. I) shows smaller error compared to the pseudo-labels. This suggests that the model was able to generalize reducing the error.

2) *K-nearest neighbors (k-NN)*: The problem of expensive position labels is not specific to neural networks. To demonstrate the compatibility of our solution with other positioning methods, we also evaluate a k-NN regressor as a possible positioning solution. In this case, for each test sample we look up 7 neighbors using L_1 distance for CSI features from train set and take the average pseudo-labeled position. The resulting mean absolute error is $14.8 \pm 1.1 \text{ cm}$, which is close to NN result ($13.4 \pm 0.9 \text{ cm}$). Thus, our pseudo-labels approach can be applied to different downstream positioning systems.

3) *Imprecise position measurements*: We add Gaussian noise to positions to imitate noisy measurements in control points. Resulting positions and velocities are used as starting values for IMU integration. Fig. 10 shows that the accuracy degrades with noise, although additional control points from the other corners of the area help mitigate this effect. Note that the velocity is calculated as a discrete difference of positions and is therefore heavily distorted by noise. In real applications, more sophisticated techniques can be used to obtain a more robust velocity approximation, such as the Kalman filter.

4) *Control points*: The choice of control points has significant impact on the final model accuracy. If there are few control points, the trajectory between them is too long and the IMU measurements accumulate the error. In the main

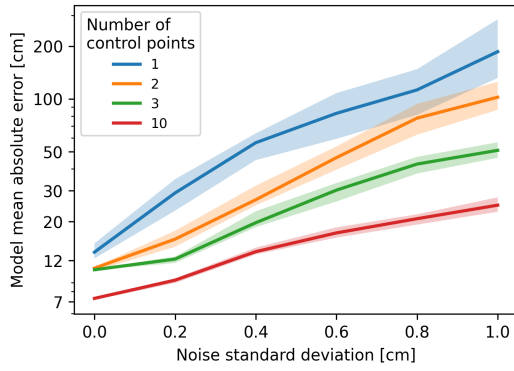


Fig. 10. Dependency between IMU-supervised model accuracy and positions noise for Warehouse dataset. The light area is 0.1 and 0.9 quantiles, the line is median for 30 seeds. Vertical axis is in logarithmic scale.

experiment, we use one control point at starting position with 20 cm radius. In this case, our dataset is represented as 35 subtrajectories between control points with median length of 51 m. Additionally, we demonstrate the accuracy for random control points with radius 1 cm, 5 cm and 10 cm on Fig. 11. Note that control points are spread uniformly, which is the best setting for Channel Charting method. Nevertheless, it can be seen that IMU supervision provides a much stronger signal.

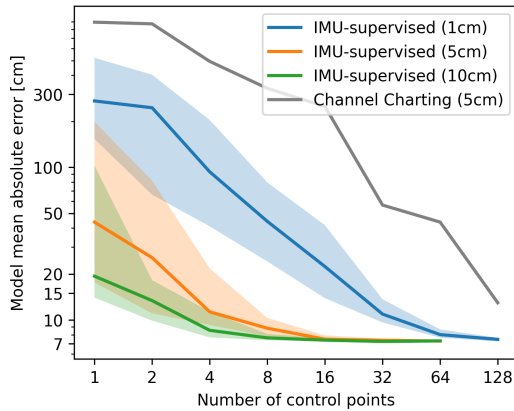


Fig. 11. Dependency between model accuracy and the control points with different radius for Warehouse dataset. The light area is 0.1 and 0.9 quantiles, the line is the median for 30 seeds. Both axes are in logarithmic scale.

TABLE III
IMUSENSOR CONFIGURATION

TemperatureScaleFactor	0.008	$\% \text{ } ^\circ\text{C}^{-1}$
ConstantBias	0.1962	m s^{-2}
TemperatureBias	0.0014715	$\text{m s}^{-2} \text{ } ^\circ\text{C}^{-1}$
NoiseDensity	0.0012361	$\text{m/s}^2/\sqrt{\text{Hz}}$

V. CONCLUSION

Localization is an important task, which raises several challenges. Often, specific equipment, such as Lidar, is not available. Moreover, common sources of information, such as

visual observations, may not preserve privacy. The use of 5G signal indoor is widespread and CSI-based localization has emerged as a supervised learning task. In this work, we have addressed the bottleneck of such methods, the dependency on hard-to-acquire position labels. We have introduced the practical algorithm to obtain pseudo-labels from IMU measurements and confirmed our findings with empirical results. Our method demonstrates high accuracy (9.4 cm mean absolute error) for actual measurements.

REFERENCES

- [1] J. A. del Peral-Rosado, R. Raulefs, J. A. López-Salcedo, and G. Seco-Granados, "Survey of cellular mobile radio localization methods: From 1g to 5g," *IEEE Communications Surveys & Tutorials*, vol. 20, no. 2, pp. 1124–1148, 2017.
- [2] V. Savic and E. G. Larsson, "Fingerprinting-based positioning in distributed massive mimo systems," in *2015 IEEE 82nd vehicular technology conference (VTC2015-Fall)*. IEEE, 2015, pp. 1–5.
- [3] A. Khalajmehrabadi, N. Gatsis, and D. Akopian, "Modern wlan fingerprinting indoor positioning methods and deployment challenges," *IEEE Communications Surveys & Tutorials*, vol. 19, no. 3, pp. 1974–2002, 2017.
- [4] J. Liu, N. Liu, Z. Pan, and X. You, "Autloc: Deep autoencoder for indoor localization with rss fingerprinting," in *2018 10th International Conference on Wireless Communications and Signal Processing (WCSP)*. IEEE, 2018, pp. 1–6.
- [5] J. Vieira, E. Leitinger, M. Sarajlic, X. Li, and F. Tufvesson, "Deep convolutional neural networks for massive mimo fingerprint-based positioning," in *2017 IEEE 28th Annual International Symposium on Personal, Indoor, and Mobile Radio Communications (PIMRC)*. IEEE, 2017, pp. 1–6.
- [6] M. Arnold, J. Hoydis, and S. ten Brink, "Novel massive mimo channel sounding data applied to deep learning-based indoor positioning," in *SCC 2019; 12th International ITG Conference on Systems, Communications and Coding*. VDE, 2019, pp. 1–6.
- [7] C. Studer, S. Medjkouh, E. Gonultaş, T. Goldstein, and O. Tirkkonen, "Channel charting: Locating users within the radio environment using channel state information," *IEEE Access*, vol. 6, pp. 47 682–47 698, 2018.
- [8] I. Karmanov, F. G. Zanjani, I. Kadampot, S. Merlin, and D. Dijkman, "Wicluster: Passive indoor 2d/3d positioning using wifi without precise labels," in *2021 IEEE Global Communications Conference (GLOBECOM)*. IEEE, 2021, pp. 1–7.
- [9] F. Ghazvinian Zanjani, I. Karmanov, H. Ackermann, D. Dijkman, S. Merlin, M. Welling, and F. Porikli, "Modality-agnostic topology aware localization," *Advances in Neural Information Processing Systems*, vol. 34, pp. 10 457–10 468, 2021.
- [10] K. S. Gill, S. Nguyen, M. M. Thein, and A. M. Wyglinski, "Three-way deep neural network for radio frequency map generation and source localization," *arXiv preprint arXiv:2111.12175*, 2021.
- [11] S. Kadambi, A. Behboodi, J. B. Soriaga, M. Welling, R. Amiri, S. Yerramalli, and T. Yoo, "Neural rf slam for unsupervised positioning and mapping with channel state information," in *ICC 2022-IEEE International Conference on Communications*. IEEE, 2022, pp. 3238–3244.
- [12] M. Arnold and M. Alloulah, "Benchmarking learnt radio localisation under distribution shift," *arXiv preprint arXiv:2210.01930*, 2022.
- [13] C. Yang, Z. Cheng, X. Jia, L. Zhang, L. Li, and D. Zhao, "A novel deep learning approach to 5g csi/geomagnetism/vio fused indoor localization," *Sensors*, vol. 23, no. 3, p. 1311, 2023.
- [14] J. Yu, P. Wang, T. Koike-Akino, and P. V. Orlik, "Multi-modal recurrent fusion for indoor localization," in *ICASSP 2022-2022 IEEE International Conference on Acoustics, Speech and Signal Processing (ICASSP)*. IEEE, 2022, pp. 5083–5087.
- [15] B. Zhang, H. Sifaou, and G. Y. Li, "Csi-fingerprinting indoor localization via attention-augmented residual convolutional neural network," *IEEE Transactions on Wireless Communications*, 2023.
- [16] K. Long, D. F. Nsalo Kong, K. Zhang, C. Tian, and C. Shen, "A csi-based indoor positioning system using single uwb ranging correction," *Sensors*, vol. 21, no. 19, p. 6447, 2021.
- [17] Remcom. (2022) Wireless insite. [Online]. Available: <https://www.remcom.com/wireless-insite-em-propagation-software>